PERGAMON

Mechatronics 12 (2002) 595–616

MECHATRONICS

Adaptive robust motion control of linear motors for precision manufacturing

Bin Yao *, Li Xu

School of Mechanical Engineering, Purdue University, West Lafayette, IN 47907, USA

Received 6 October 1999; accepted 11 October 2000

Abstract

Linear motors offer several advantages over their rotary counterparts in many precision manufacturing applications requiring linear motion; linear motors can achieve a much higher speed and have the potential of gaining a higher load positioning accuracy due to the elimination of mechanical transmission mechanisms. However, these advantages are obtained at the expense of added difficulties in controlling such a system. Specifically, linear motors are more sensitive to disturbances and parameter variations. Furthermore, certain types of linear motors such as the iron core are subject to significant nonlinear effects due to periodic cogging force and force ripple. To address all these issues, the recently proposed adaptive robust control (ARC) strategy is applied and a discontinuous projection-based ARC controller is constructed. In particular, based on the special structures of various periodic nonlinear forces, design models consisting of known basis functions with unknown weights are used to approximate those unknown nonlinear forces. On-line parameter adaptation is then utilized to reduce the effect of various parametric uncertainties such as unknown weights, inertia, and motor parameters while certain robust control laws are used to handle the uncompensated uncertain nonlinearities effectively for high performance. The resulting ARC controller achieves a guaranteed transient performance and a guaranteed final tracking accuracy in the presence of both parametric uncertainties and uncertain nonlinearities. In addition, in the presence of parametric uncertainties, the controller achieves asymptotic output tracking. Extensive simulation results are shown to illustrate the effectiveness of the proposed algorithm.

Keywords: Linear motor; Precision motion control; Adaptive control; Robust control; Servo control

* Corresponding author. Tel.: +1-765-494-7746; fax: +1-765-494-0539.
E-mail address: byao@ecn.purdue.edu (Bin Yao).

0957-4158/02/$ - see front matter
PII: S0957-4158(01)00008-3

1. Introduction

Modern mechanical systems, such as machine tools, semiconductor manufacturing equipment, and automatic inspection machines, often require high-speed/high-accuracy linear motions. These linear motions are usually realized using rotary motors with mechanical transmission mechanisms such as reduction gears and lead screw. Such mechanical transmissions not only significantly reduce linear motion speed and dynamic response, but also introduce backlash, large frictional and inertial loads, and structural flexibility. Backlash and structural flexibility physically limit the accuracy that any control system can achieve. As an alternative, direct-drive linear motors, which eliminate the use of mechanical transmissions, show promise for widespread use in high-speed/high-accuracy positioning systems [1–3]. In general, the linear motor has the following advantages over its rotary-motor counterpart: (a) no backlash and less friction, resulting in very high accuracy; (b) no mechanical limitations on achievable accelerations and velocities; achievable velocities are only limited by the encoder bandwidth or by the power electronics; (c) bandwidths are only limited by encoder resolution, measurement noise, calculation time, and frame stiffness; and (d) mechanical simplicity, higher reliability, and longer lifetime.

The direct-drive linear motor gains high-speed/high-accuracy potential by eliminating mechanical transmission [1–3]. However, it also loses the advantage of using mechanical transmissions – gear reduction reduces the effect of model uncertainties such as parameter variations (e.g., uncertain payloads) and external disturbance (e.g., cutting forces in machining). Furthermore, certain types of linear motors such as the iron core have significant uncertain nonlinearities due to electromagnetic force ripple and magnetic cogging force [3]. These uncertain nonlinearities are directly transmitted to the load and thus have significant effect on the motion of the load. Thus, in order for a linear motor system to be able to function and to deliver its high performance potential, a controller which can achieve the required high accuracy in spite of various parametric uncertainties and uncertain nonlinear effects, has to be employed.

A great deal of effort has been devoted to solving the difficulties in controlling linear motors [1–6]. In [1], Alter and Tsao presents a comprehensive design approach for the control of linear motor-driven machine tool axes. H_∞ optimal feedback control is used to provide high dynamic stiffness to external disturbances (e.g., cutting forces in machining). Feedforward is also introduced in [2] to improve tracking performance. Practically, H_∞ design may be conservative for high-speed/high-accuracy tracking control and there is no systematic way to translate practical information about plant uncertainty and modeling inaccuracy into quantitative terms that allow the application of H_∞ techniques. In [4], a disturbance compensation method based on disturbance observer (DOB) [5,7] was proposed to make the linear motor system robust to model uncertainties. It was shown both theoretically and experimentally in [8] that the DOB design may not handle discontinuous disturbances such as Coulomb friction well and cannot deal with large extent of parametric uncertainties. To reduce the nonlinear effect of force ripple and cogging force, in [3], feedforward compensation terms, which are based on an off-line

experimentally identified model of first-order approximation of ripple force, were added to the position controller. Since not all magnets in a linear motor and not all linear motors of the same type are identical, feedforward compensation based on off-line identification model may be too sensitive and costly to be useful. In [6], a neural-network-based learning feedforward controller was proposed to reduce positional inaccuracy due to reproducible ripple forces or any other reproducible and slowly varying disturbances over different runs of the same desired trajectory (or repetitive tasks). However, overall closed-loop stability is not guaranteed. In fact, it was observed in [6] that instability may occur at high-speed movements. Furthermore, learning process may take too long to be useful due to the use of a small adaptation rate for stability.

In [9–12], Yao and Tomizuka proposed an adaptive robust control (ARC) approach for the high-performance robust control of uncertain nonlinear systems in the presence of both parametric uncertainties and uncertain nonlinearities. The approach effectively combines the design techniques of adaptive control (AC) [13,14] and those of deterministic robust control (DRC) [15,16] (e.g., sliding mode control, SMC) and improves performance by preserving the advantages of both AC and DRC. Comparative experimental results for trajectory tracking control of robot manipulators [10] have shown the advantages of the proposed ARC and the improvement of performance. A general theoretical framework is recently formalized by Yao in [17].

In [8], the ARC approach is applied to the high-speed/high-accuracy motion control of machine tools driven by conventional AC rotary motors. Comparative experimental results obtained on a Matsuura 510 V SS high-speed machining center show that compared to a conventional DOB design, the proposed ARC results in better handling of the discontinuous disturbances and the improvement of overall tracking performance. Large parameter variation, such as the variation of inertia, is also allowed in the ARC design as in contrast to the limited range of parameter variation that the DOB can handle. In addition, ARC has a better ability in dealing with the control saturation problem since the ARC design has a built-in anti-integration windup mechanism.

This paper generalizes the ARC approach to the high-speed/high-accuracy motion control of iron-core linear motors. In addition to the conventional design difficulties due to large variation of inertia load, unknown friction, and disturbance forces, there are several particular problems associated with the control of iron-core linear motors. First, different from other types of linear motors such as epoxy-core linear motors, the iron-core linear motors have a large magnitude of ripple forces and the effect of these nonlinear ripple forces has to be considered in the controller design stage (e.g., the LCK-type linear motors in [18]). Second, the electrical time constant of the internal current feedback loop for an iron-core linear motor is not so small due to the large inductance associated with the iron core. Thus, the electrical current feedback loop cannot be neglected in the controller design stage as opposed to the control of conventional machine tools in [8]. This added electrical dynamics increases the controller design difficulties significantly since the resulting system is of higher "relative degree" [11] and backstepping design [14] via ARC Lyapunov functions

[12,17] has to be employed. Third, due to variations of the inertia load and the motor force constant, parametric uncertainties will appear in the input channels of the intermediate design steps. This further complicates the problem and prohibits the direct application of the discontinuous projection-based ARC backstepping design in [17]. All these issues will be addressed in the paper. An ARC controller that can handle various parametric uncertainties as well as uncertain nonlinearities will be constructed. The paper thus advances the control of linear motors considerably since none of the published papers deal with all these aspects all together at once. In addition, the proposed ARC controller is able to achieve a guaranteed transient as well as final tracking accuracy in general while being able to achieve asymptotic output tracking in the presence of parametric uncertainties. Various simulation results will be shown to illustrate the effectiveness of the proposed method.

The paper is organized as follows. Dynamic model of iron-core linear motors is presented in Section 2. The proposed ARC controller is shown in Section 3. Simulation results are presented in Section 4, and conclusions are drawn in Section 5.

2. Problem formulation and dynamic models

An iron-core brushless DC linear motor (LCK series in [18]) is shown in Fig. 1. It consists of a permanent magnet stator, a translator (the counterpart of the rotor in a rotary motor) formed by a number of iron-core coils and a Hall effect position sensor mounted on the translator. Essentially, the motor is a synchronous permanent magnet motor with electronic commutation. The goal is to have the inertia load mounted on the translator track any specified motion trajectory as closely as possible; examples like a machine tool axis [8] and the load-carrying systems.

The dynamic equation of the inertia load can be described by

$$M\ddot{x}_L = F_{\mathrm{m}} - B\dot{x}_L + f_{\mathrm{friction}}(\dot{x}_L) + f_{\mathrm{dis}}(t, x_L, \dot{x}_L), \tag{1}$$

where x_L represents the displacement of the inertia load, M is the mass of the inertia load plus the iron-core translator, F_{m} is the total electromagnetic force generated by the linear motor, B is the combined coefficient of the damping and viscous friction on the load, f_{friction} represents the combination of stiction and Coulomb friction, and $f_{\mathrm{dis}}(t, x_L, \dot{x}_L)$ represents the external disturbances such as cutting force in machining. A simple mathematical model for friction f_{friction} that takes into account of stiction, Coulomb friction, and Stribeck effect can be written as [19,20]

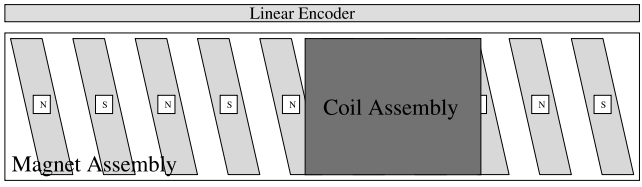

Fig. 1. An iron-core brushless DC linear motor system.

$$f_{\text{friction}}(\dot{x}_L) = -[f_c + (f_s - f_c)\,e^{-|\dot{x}_L/\dot{x}_s|^{\xi}}]\text{sgn}(\dot{x}_L), \tag{2}$$

where f_s is the level of static friction, f_c is the minimum level of Coulomb friction, and $\dot{x}_s$ and ξ are empirical parameters used to describe the Stribeck effect.

For the application studied, an analog power amplifier with built-in electronic commutation is used to generate the three-phase voltages necessary to drive the linear motor's three-phase motor windings to produce the needed electromagnetic force F_m. Without going into the details of the working mechanisms of the amplifier and the motor, a popular simplified model that relates the generated F_m to the control input voltage u of the amplifier is given by [21]

$$\begin{aligned} &F_m = K_{F_0} i, \\ &L\frac{d}{dt} i + iR + K_E \dot{x}_L = u, \end{aligned} \tag{3}$$

where K_{F_0} is the average force constant, i is the motor current amplitude, R and L are the armature resistance and inductance, respectively, and K_E is the electromotive force coefficient. Such a simplified model has been successfully used by many researchers in the control of rotary motors and certain types of linear motors [22].

For iron-core linear motors, the simplified linear motor model Eq. (3) may not be sufficient since iron-core linear motors have relatively larger magnitude of nonlinear *cogging force* and *force ripple*, which are neglected in the simplified model Eq. (3). These nonlinear forces are generated due to the particular structure of the iron-core linear motors [3,6,23]:

- *Cogging* or *dentent force* is a magnetic force developed due to the attraction between the permanent magnets and the iron cores of the translator. It depends only on the relative position of the motor coils with respect to the magnets, and is independent of the motor current. Thus, this force can be described as a position-dependent function $f_{\text{cogging}}(x_L)$. If the permanent magnets of the same linear motor are all identical and are equally spaced at a pitch of P, then, $f_{\text{cogging}}(x_L)$ is a periodic function with a period of P, i.e. $f_{\text{cogging}}(x_L + P) = f_{\text{cogging}}(x_L)$, which is assumed in the paper.
- *Force ripple* is developed due to the periodic variation of the force constant; when the position of the translator (or load) changes, the winding self-inductance varies, which in turn results in the variation of the force constant. Thus, when current flows through the coils, a position-dependent periodic force is resulted. To take this effect into account, a position-dependent term can be added to modify the force constant in Eq. (3) to $K_F(x_L) = K_{F_0} + K_{F_x}(x_L)$, in which $K_{F_x}(x_L)$ is a periodic function with a period of P, i.e. $K_{F_x}(x_L + P) = K_{F_x}(x_L)$.

By taking into account the effect of cogging force and force ripple, the motor force is given by

$$F_m = K_F(x_L) i + f_{\text{cogging}}(x_L), \quad K_F(x_L) = K_{F_0} + K_{F_x}(x_L), \tag{4}$$

where i is related to the control input u by Eq. (3). Defining the position, velocity, and current as the state variables, i.e. $x = [x_1, x_2, x_3]^T \triangleq [x_L, \dot{x}_L, i]^T$, from Eqs. (1), (3) and (4), the entire system can be expressed in state space form as:

$$\begin{aligned}\dot{x}_1 &= x_2,\\ \dot{x}_2 &= \frac{1}{M}\left[(K_{F_0} + K_{F_x}(x_1))x_3 - Bx_2 + f_{\text{friction}}(x_2) + f_{\text{cogging}}(x_1) + f_{\text{dis}}(t, x_1, x_2)\right],\\ \dot{x}_3 &= -\frac{R}{L}x_3 - \frac{K_E}{L}x_2 + \frac{1}{L}u.\end{aligned} \tag{5}$$

Given the desired motion trajectory $x_{Ld}(t)$, the objective is to synthesize a control input u such that the output $y = x_1$ tracks $x_{Ld}(t)$ as closely as possible in spite of various model uncertainties.

Remark 1. If not considered in the design, cogging force and force ripple can be thought of as external disturbances which vary with the translator position, and thus cause tracking errors. At very high speeds, they are of high frequency and are usually filtered out by the system inertia. But at low speeds, they produce noticeable effects that may not be tolerable [3,6]. ♢

3. ARC of linear motor systems

In this section, the ARC strategy recently developed in [11,17,24] will be adopted to solve the above control problem due to the performance-oriented design philosophy and the strong performance robustness of the ARC controllers to model uncertainties. The section is organized as follows. The physical models presented in Section 2 will be first transformed into some models suitable for controller design in Section 3.1. The proposed ARC controller is then detailed in Section 3.2. Finally, the desired trajectory initialization and generation are employed for a guaranteed transient performance in general, which is detailed in Section 3.3.

3.1. Design models and assumptions

To start the controller design, practical and reasonable assumptions on the system have to be made. As we discussed in Section 2, iron-core linear motor is subject to various parametric uncertainties, external disturbances, and largely reproducible nonlinearities such as cogging, force ripple, and friction force. For the reproducible cogging, force ripple, and friction force, although feedforward compensation techniques based on off-line identified models can be used to cancel their effects (e.g., force ripple compensation in [3] and friction compensation in [25]), such a procedure may be time-consuming and sometimes may not be so practical since they cannot handle the variations among different motors and different runs. In the following, instead of using these off-line techniques, based on the structural properties of these reproducible nonlinear forces, we will use some simple models with unknown weights to approximate them; the unknown weights will be adjusted on-line via certain parameter adaptation laws to achieve an improved model compensation and the model approximation error will be handled via certain robust control laws to achieve a guaranteed robust performance. Specifically, since $f_{\text{cogging}}(x_1)$ and $K_{F_x}(x_1)$

are periodic functions with a known period P, they can be approximated quite accurately by their first several harmonics, which are denoted as $\bar{f}_{\text{cogging}}(x_1)$ and $\bar{K}_{F_x}(x_1)$, respectively and represented by

$$\begin{aligned}\bar{f}_{\text{cogging}}(x_1) &= A_c^T S_c(x_1),\\ \bar{K}_{F_x}(x_1) &= A_K^T S_K(x_1),\end{aligned} \tag{6}$$

where $A_c = [A_{c1s}, A_{c1c}, \ldots, A_{cq_1s}, A_{cq_1c}]^T \in R^{2q_1}$ and $A_K = [A_{K1s}, A_{K1c}, \ldots, A_{Kq_2s}, A_{Kq_2c}]^T \in R^{2q_2}$ are the unknown weights, $S_c(x_1) = [\sin((2\pi/P)x_1), \cos((2\pi/P)x_1), \ldots, \sin((2\pi q_1/P)x_1), \cos((2\pi q_1/P)x_1)]^T$ and $S_K(x_1) = [\sin((2\pi/P)x_1), \cos((2\pi/P)x_1), \ldots, \sin((2\pi q_2/P)x_1), \cos((2\pi q_2/P)x_1)]^T$ are the known basis shape functions, and q_1 and q_2 are the numbers of harmonics used for compensation. The larger q_1 and q_2 are, the better $\bar{f}_{\text{cogging}}(x_1)$ and $\bar{K}_{F_x}(x_1)$ approximate $f_{\text{cogging}}(x_1)$ and $K_{F_x}(x_1)$, but the larger the number of parameters to be adapted. So a trade-off has to be made based on the particular structure of a motor. For example, in [3], it was experimentally observed that the first and the third harmonics are sufficient for approximation.

The friction model (2) is discontinuous at $\dot{x}_1 = 0$. Thus one cannot use the model (2) for friction compensation since, as evident from (5), one cannot generate a discontinuous motor force to accomplish the job. To by-pass this technical difficulty, we will use a simple continuous friction model to approximate the actual discontinuous friction model (2) for model compensation; the model used in the paper is represented by $\bar{f}_{\text{friction}} = A_f S_f(x_2)$, where the amplitude A_f may be known or unknown, and $S_f(x_2)$ may be chosen as any differentiable function which approximates the shape of friction curve well. The second equation of (5) can thus be written as:

$$\dot{x}_2 = \frac{1}{M}\left[(K_{F_0} + A_K^T S_K(x_1))x_3 - Bx_2 + A_f S_f(x_2) + A_c^T S_c(x_1) + \tilde{f}(t, x_1, x_2, x_3)\right], \tag{7}$$

where $\tilde{f}$ represents the lumped external disturbances and model approximation errors and is given by

$$\tilde{f} = (K_{F_x}(x_1) - \bar{K}_{F_x}(x_1))x_3 + (f_{\text{friction}} - \bar{f}_{\text{friction}}) + (f_{\text{cogging}} - \bar{f}_{\text{cogging}}) + f_{\text{dis}}(t, x_1, x_2). \tag{8}$$

In general, the system is subjected to parametric uncertainties due to the variations of M, B, A_c, A_K, A_f, K_E, L, R, and the nominal value of the lumped disturbance $\tilde{f}$, $\tilde{f}_n$. In order to use parameter adaptation to reduce parametric uncertainties to improve performance, it is necessary to linearly parameterize the state space equations in terms of a set of unknown parameters. For this purpose, define the unknown parameter set θ as $\theta = [\theta_1, \theta_{2b}, \theta_3, \theta_4, \theta_{5b}, \theta_6, \theta_7, \theta_8, \theta_9]^T \in R^{p=7+2q_1+2q_2}$ as $\theta_1 = K_{F_0}/M$, $\theta_{2b} = (1/M)A_K \in R^{2q_1}$, $\theta_3 = -B/M$, $\theta_4 = A_f/M$, $\theta_{5b} = (1/M)A_c \in R^{2q_2}$, $\theta_6 = \tilde{f}_n/M$, $\theta_7 = 1/L$, $\theta_8 = -R/L$, and $\theta_9 = -K_E/L$. The state space Eqs. (5) and (7) can thus be linearly parameterized in terms of θ as

$$\begin{aligned}\dot{x}_1 &= x_2,\\ \dot{x}_2 &= \left[\theta_1 + \theta_{2b}^T S_K(x_1)\right]x_3 + \theta_3 x_2 + \theta_4 S_f(x_2) + \theta_{5b}^T S_c(x_1) + \theta_6 + \tilde{d},\\ \dot{x}_3 &= \theta_8 x_3 + \theta_9 x_2 + \theta_7 u,\end{aligned} \tag{9}$$

where $\tilde{d}(t,x_1,x_2,x_3) = (1/M)[\tilde{f} - \tilde{f}_n]$ represents the uncompensated disturbances and modeling errors. For simplicity, the following notations will be used: $\bullet_i$ for the ith component of the vector $\bullet$, $\bullet_{\min}$ for the minimum value of $\bullet$, and $\bullet_{\max}$ for the maximum value of $\bullet$. The operation $<$ for two vectors is performed in terms of the corresponding elements of the vectors. The following practical assumptions are made:

Assumption A1. The extents of the parametric uncertainties and uncertain nonlinearities are known, i.e.,

$$\begin{aligned} &\theta \in \Omega_\theta \triangleq \{\theta : \theta_{\min} < \theta < \theta_{\max}\}, \\ &|\tilde{d}| \leqslant \delta_d(t,x_1,x_2) \end{aligned} \tag{10}$$

where $\theta_{\min} = [\theta_{1\min}, \theta_{2b\min}, \ldots, \theta_{9\min}]^T$, $\theta_{\max} = [\theta_{1\max}, \ldots, \theta_{9\max}]^T$, and $\delta_d(t,x_1,x_2)$ are known.

Assumption A2. $\forall \theta \in [\theta_{\min}, \theta_{\max}]$, $\bar{K}_F = \theta_1 + \theta_{2b}^T S_K(x_1)$ is positive, i.e., there exists $K_{F_{\min}} > 0$ such that $\bar{K}_F > K_{F_{\min}}$. $\diamondsuit$

Note that Assumption A2 is merely a re-phrase of the fact that the actual motor force constant K_F is positive.

3.2. Discontinuous projection-based ARC controller

Compared to the problem studied in [8], it is readily seen that the additional theoretical difficulties in controlling (9) are: (a) the relative degree from the input u to the output x_1 is *three* and the system has unmatched model uncertainties since parametric uncertainties and uncertain nonlinearities appear in equations that do not contain control input u (the second Eq. (9)); and (b) input or virtual input channels of each design step have parametric uncertainties, i.e., the term $(\theta_1 + \theta_{2b}^T S_K(x_1))x_3$ in the second Eq. (9) and the term $\theta_7 u$ in the third equation contain parametric uncertainties. Both difficulties increase the controller design complexity significantly. In principle, both difficulties may be solved by applying the ARC strategies in [11,12]. However, the design in [11,12] is based on the tuning function-based adaptive backstepping design [14], which needs to incorporate the adaptation law in the design of control functions at each step. As a result, smooth projections have to be used to solve the design conflicts between adaptive control technique and robust control technique, which is technical and may not be so convenient for practical implementation. Here, instead of using the smooth projection, the widely used discontinuous projection method in adaptive systems [26,27] will be used to solve the conflicts between the robust control design and adaptive control design. This type of ARC strategy has been developed in [17] for higher relative degree SISO nonlinear systems in a semi-strict feedback form. However, the form in [17] does not allow model uncertainties in the input (or virtual input) channels of each design step, which is not the case considered here due to the

appearance of parametric uncertainties in the virtual input channel of the second Eq. (9) (i.e., the term $(\theta_1 + \theta_{2b}^T S_K(x_1))x_3$) and the term $\theta_7 u$ in the last step. Thus, the following design will also advance the theory of the discontinuous projection-based ARC design.

3.2.1. Notations and discontinuous projection

Let $\hat{\theta}$ denote the estimate of θ and $\tilde{\theta}$ the estimation error (i.e., $\tilde{\theta} = \hat{\theta} - \theta$). Viewing (10), a simple discontinuous projection can be defined [26,27] as

$$\mathrm{Proj}_{\hat{\theta}}(\bullet) = \begin{cases} 0 & \text{if } \hat{\theta}_i = \theta_{i\max} \text{ and } \bullet > 0, \\ 0 & \text{if } \hat{\theta}_i = \theta_{i\min} \text{ and } \bullet < 0, \\ \bullet & \text{otherwise.} \end{cases} \tag{11}$$

By using an adaptation law given by

$$\dot{\hat{\theta}} = \mathrm{Proj}_{\hat{\theta}}(\Gamma\tau), \tag{12}$$

where $\Gamma > 0$ is a diagonal matrix, τ is an adaptation function to be synthesized later. It can be shown [9] that for any adaptation function τ, the projection mapping used in (12) guarantees

$$\begin{aligned} &(\mathbf{P1}) \qquad \hat{\theta} \in \bar{\Omega}_\theta \triangleq \{\hat{\theta} : \theta_{\min} \leqslant \hat{\theta} \leqslant \theta_{\max}\}, \\ &(\mathbf{P2}) \qquad \tilde{\theta}^T(\Gamma^{-1}\mathrm{Proj}_{\hat{\theta}}(\Gamma\tau) - \tau) \leqslant 0, \qquad \forall\tau. \end{aligned} \tag{13}$$

3.2.2. Controller design

The design parallels the recursive backstepping design procedure via ARC Lyapunov functions in [12,17] as follows.

3.2.2.1. Step 1. Noting that the first equation of (9) does not have any uncertainties, an ARC Lyapunov function can thus be constructed for the first two equations of (9) directly. Define a switching-function-like quantity as

$$z_2 = \dot{e}_1 + k_p e_1 = x_2 - x_{2eq}, \qquad x_{2eq} \triangleq \dot{x}_{1d} - k_p e_1, \tag{14}$$

where $e_1 = x_1 - x_{1d}(t)$, in which the desired trajectory $x_{1d}(t)$ will be specified later to achieve a guaranteed transient performance, k_p is any positive feedback gain. If z_2 is small or converges to zero exponentially, then the output tracking error e_1 will be small or converge to zero exponentially since $G_s(s) = e_1(s)/z_2(s) = 1/(s + k_p)$ is a stable transfer function. So the rest of the design is to make z_2 as small as possible with a guaranteed transient performance. Differentiating (14) and noting (9)

$$\dot{z}_2 = \dot{x}_2 - \dot{x}_{2eq} = \bar{K}_F x_3 + \theta_3 x_2 + \theta_4 S_f(x_2) + \theta_{5b}^T S_c(x_1) + \theta_6 + \tilde{d} - \dot{x}_{2eq}, \tag{15}$$

where $\dot{x}_{2eq} \triangleq \ddot{x}_{1d} - k_p \dot{e}_1$. In (15), if we treat x_3 as the input, we can synthesize a virtual control law α_2 for x_3 such that z_2 is as small as possible. Since (15) has both parametric uncertainties θ and uncertain nonlinearity $\tilde{d}$, the ARC approach proposed in [17] will be generalized to accomplish the objective.

The control function α_2 consists of two parts given by

$$\begin{aligned}&\alpha_2(x_1,x_2,\hat{\theta},t)=\alpha_{2a}+\alpha_{2s},\\&\alpha_{2a}=\frac{1}{\hat{K}_F}\Big\{-\hat{\theta}_3x_2-\hat{\theta}_4S_f(x_2)-\hat{\theta}_{5b}^TS_c(x_1)-\hat{\theta}_6+\dot{x}_{2eq}\Big\},\end{aligned}\tag{16}$$

where $\hat{K}_F=\hat{\theta}_1+\hat{\theta}_{2b}^TS_K(x_1)$ is the estimated motor force constant, α_{2a} functions as an adaptive control law used to achieve an improved model compensation through on-line parameter adaptation given by (12), and α_{2s} is a robust control law to be synthesized later. Noting P1 of (13) and Assumption A2, $\hat{K}_F>0$. Thus the control function (16) is well defined no matter what type of adaptation function to be used. Let $z_3=x_3-\alpha_2$ denote the input discrepancy. Substituting (16) into (15) leads to

$$\begin{aligned}\dot{z}_2&=\bar{K}_F(z_3+\alpha_{2s})+\hat{K}_F\alpha_{2a}-\tilde{K}_F\alpha_{2a}+\theta_3x_2+\theta_4S_f(x_2)+\theta_{5b}^TS_c(x_1)+\theta_6+\tilde{d}-\dot{x}_{2eq}\\&=\bar{K}_F(z_3+\alpha_{2s})-\tilde{\theta}^T\phi_2+\tilde{d},\end{aligned}\tag{17}$$

where $\phi_2\overset{\Delta}{=}[\alpha_{2a},S_K^T(x_1)\alpha_{2a},x_2,S_f(x_2),S_c^T(x_1),1,0,0,0]^T$. In the tuning function-based backstepping adaptive control [14], the key point is to incorporate the adaptation function (or tuning function) in the construction of control functions to compensate the destabilizing effect of the time-varying adaptation law. Here, due to the use of discontinuous projection (11), the adaptation law (12) is discontinuous and thus *cannot* be used in the control law design at each step since backstepping design needs the control function synthesized at each step to be sufficiently smooth in order to obtain its partial derivatives. In the following, it will be shown that this design difficulty can be overcome by strengthening the robust control law design.

The robust control function α_{2s} consists of two terms given by

$$\alpha_{2s}=\alpha_{2s1}+\alpha_{2s2},\qquad \alpha_{2s1}=-\frac{1}{K_{F\min}}k_{2s1}z_2,\tag{18}$$

where α_{2s2} is a robust control function designed in the following and k_{2s1} is any nonlinear feedback gain satisfying

$$k_{2s1}\geqslant\|C_{\phi_2}\Gamma\phi_2\|^2+k_2,\qquad k_2>0\tag{19}$$

in which C_{ϕ_2} is a positive definite constant diagonal matrix to be specified later and k_2 is a positive design parameter. Substituting (18) into (17),

$$\dot{z}_2=\bar{K}_F(x_1)z_3-\frac{\bar{K}_F(x_1)}{K_{F\min}}k_{2s1}z_2+\bar{K}_F(x_1)\alpha_{2s2}-\tilde{\theta}^T\phi_2+\tilde{d}.\tag{20}$$

Define a positive semi-definite (psd) function V_2 as $V_2=(1/2)w_2z_2^2$ where $w_2>0$ is a weighting factor. From (20), its time derivative is

$$\dot{V}_2=\bar{K}_F(x_1)w_2z_2z_3-w_2\frac{\bar{K}_F(x_1)}{K_{F\min}}k_{2s1}z_2^2+w_2z_2\Big\{\bar{K}_F(x_1)\alpha_{2s2}-\tilde{\theta}^T\phi_2+\tilde{d}\Big\}.\tag{21}$$

The robust control function α_{2s2} is now chosen to satisfy the following conditions:

$$\begin{aligned}&\text{condition (i)}\quad z_2\Big\{\bar{K}_F(x_1)\alpha_{2s2}-\tilde{\theta}^T\phi_2+\tilde{d}\Big\}\leqslant\varepsilon_2,\\&\text{condition (ii)}\quad z_2\alpha_{2s2}\leqslant 0,\end{aligned}\tag{22}$$

where ε_2 is a design parameter which can be arbitrarily small. Essentially, condition (i) of (22) shows that α_{2s2} is synthesized to dominate the model uncertainties coming from both parametric uncertainties $\tilde{\theta}$ and uncertain nonlinearities $\tilde{d}$, and condition (ii) is to make sure that α_{2s2} is dissipating in nature so that it does not interfere with the functionality of the adaptive control part α_{2a}.

Remark 2. One smooth example of α_{2s2} satisfying (22) can be found in the following way. Let h_2 be any smooth function satisfying $h_2 \geqslant \|\theta_M\|^2\|\phi_2\|^2 + \delta_d^2$ where $\theta_M = \theta_{\max} - \theta_{\min}$. Then, α_{2s2} can be chosen as

$$\alpha_{2s2} = -\frac{h_2}{2K_{F\min}\varepsilon_2} z_2. \tag{23}$$

It can be shown that (22) is satisfied [11]. Other examples of α_{2s2} can be found in [9,11,17]. $\diamondsuit$

3.2.2.2. Step 2. Noting the last Eq. (9), *Step* 2 is to synthesize an actual control law for u such that i tracks the desired control function α_2 synthesized in *Step* 1 with a guaranteed transient performance, which can be done by using the same ARC design techniques as in *Step* 1. From (16) and (9),

$$\dot{\alpha}_2 = \frac{\partial \alpha_2}{\partial x_1} x_2 + \frac{\partial \alpha_2}{\partial x_2}\dot{x}_2 + \frac{\partial \alpha_2}{\partial \hat{\theta}}\dot{\hat{\theta}} + \frac{\partial \alpha_2}{\partial t} = \dot{\alpha}_{2c} + \dot{\alpha}_{2u}, \tag{24}$$

where

$$\begin{aligned}
\dot{\alpha}_{2c} &= \frac{\partial \alpha_2}{\partial x_1} x_2 + \frac{\partial \alpha_2}{\partial x_2}\left\{\hat{K}_F x_3 + \hat{\theta}_3 x_2 + \hat{\theta}_4 S_f(x_2) + \hat{\theta}_{5b}^T S_c(x_1) + \hat{\theta}_6\right\} + \frac{\partial \alpha_2}{\partial t}, \\
\dot{\alpha}_{2u} &= \frac{\partial \alpha_2}{\partial x_2}\left\{ -\left[\tilde{\theta}_1 + \tilde{\theta}_{2b}^T S_K(x_1)\right] x_3 - \tilde{\theta}_3 x_2 - \tilde{\theta}_4 S_f(x_2) - \tilde{\theta}_{5b}^T S_c(x_1) - \tilde{\theta}_6 + \tilde{d}\right\} + \frac{\partial \alpha_2}{\partial \hat{\theta}}\dot{\hat{\theta}}.
\end{aligned} \tag{25}$$

In (24), $\dot{\alpha}_{2c}$ is calculable and can be used in the design of control functions but $\dot{\alpha}_{2u}$ cannot due to various uncertainties. Therefore, $\dot{\alpha}_{2u}$ has to be dealt with in this step design. From (9),

$$\dot{z}_3 = \dot{x}_3 - \dot{\alpha}_2 = \theta_8 x_3 + \theta_9 x_2 + \theta_7 u - \dot{\alpha}_{2c} - \dot{\alpha}_{2u}. \tag{26}$$

Consider the augmented psd function V given by

$$V = V_2 + \frac{1}{2} w_3 z_3^2, \qquad w_3 > 0. \tag{27}$$

Noting (21) and (26),

$$\begin{aligned}
\dot{V} &= \bar{K}_F w_2 z_2 z_3 + \dot{V}_2|_{\alpha_2} + w_3 z_3 \dot{z}_3 \\
&= \dot{V}_2|_{\alpha_2} + w_3 z_3\left\{\frac{w_2}{w_3}\bar{K}_F z_2 + \theta_8 x_3 + \theta_9 x_2 + \theta_7 u - \dot{\alpha}_{2c} - \dot{\alpha}_{2u}\right\},
\end{aligned} \tag{28}$$

where $\dot{V}_2|_{\alpha_2}$ denotes $\dot{V}_2$ under the condition that $x_3 = \alpha_2$ (or $z_3 = 0$). Similar to (16), the actual control input u to be synthesized consists of two parts given by

$$\begin{aligned} &u = u_a(x,\hat{\theta},t) + u_s(x,\hat{\theta},t)\\ &u_a = -\frac{1}{\hat{\theta}_7}\left[\frac{w_2}{w_3}\hat{K}_F z_2 + \hat{\theta}_8 x_3 + \hat{\theta}_9 x_2 - \dot{\alpha}_{2c}\right],\\ &u_s = u_{s1} + u_{s2}, \qquad u_{s1} = -\frac{1}{\theta_{7\min}} k_{3s1} z_3,\\ &k_{3s1} \geqslant k_3 + \left\| \frac{\partial \alpha_2}{\partial \hat{\theta}} C_{\theta_3} \right\|^2 + \|C_{\phi_3}\Gamma\phi_3\|^2, \end{aligned} \tag{29}$$

where $k_3 > 0$ is a constant, C_{θ_3}, and C_{ϕ_3} are positive definite constant diagonal matrices, and u_{s2} is a robust control function to be chosen later. Substituting (29) and (25) into (28) and using similar techniques as in (17)

$$\dot{V} = \dot{V}_2|_{\alpha_2} + w_3 z_3 \left\{ \theta_7 u_s - \tilde{\theta}^T \phi_3 - \frac{\partial \alpha_2}{\partial x_2}\tilde{d} - \frac{\partial \alpha_2}{\partial \hat{\theta}}\dot{\hat{\theta}} \right\}, \tag{30}$$

where ϕ_3 is defined as

$$\begin{aligned} \phi_3 = \Bigg[&\frac{w_2}{w_3} z_2 - \frac{\partial \alpha_2}{\partial x_2} x_3, S_K^T(x_1)\left(\frac{w_2}{w_3} z_2 - \frac{\partial \alpha_2}{\partial x_2} x_3\right),\\ &-\frac{\partial \alpha_2}{\partial x_2} x_2, -\frac{\partial \alpha_2}{\partial x_2} S_f(x_2), -\frac{\partial \alpha_2}{\partial x_2} S_c^T(x_1), -\frac{\partial \alpha_2}{\partial x_2}, u_a, x_3, x_2 \Bigg]^T. \end{aligned}$$

Similar to (22), the robust control function u_{s2} is chosen to satisfy

$$\begin{aligned} &\text{condition (i)} \quad z_3 \left[\theta_7 u_{s2} - \tilde{\theta}^T \phi_3 - \frac{\partial \alpha_2}{\partial x_2}\tilde{d} \right] \leqslant \varepsilon_3,\\ &\text{condition (ii)} \quad z_3 u_{s2} \leqslant 0, \end{aligned} \tag{31}$$

where ε_3 is a design parameter. As in Remark 1, one example of u_{s2} satisfying (31) is given by

$$u_{s2} = -\frac{1}{2\theta_{7\min}\varepsilon_3} h_3 z_3 \tag{32}$$

in which h_3 is any continuous function satisfying $h_3 \geqslant \|\theta_M\|^2 \|\phi_{3i}\|^2 + \delta_d^2$.

Theorem 1. *Let the parameter estimates be updated by the adaptation law* (12) *in which* τ *is chosen as*

$$\tau = w_2 \phi_2 z_2 + w_3 \phi_3 z_3. \tag{33}$$

If controller parameters $C_{\phi_2} = \mathbf{diag}\{C_{\phi_{21}}, \ldots, C_{\phi_{2p}}\}$, $C_{\phi_3} = \mathbf{diag}\{C_{\phi_{31}}, \ldots, C_{\phi_{3p}}\}$, *and* $C_{\theta_3} = \mathbf{diag}\{C_{\theta_{31}}, \ldots, C_{\theta_{3p}}\}$ *are chosen such that,* $\forall l$, $C_{\phi_{2l}} C_{\theta_{3l}} \geqslant \sqrt{(1/2) w_2 w_3}$ *and* $C_{\phi_{3l}} C_{\theta_{3l}} \geqslant \sqrt{(1/2)} w_3$, *where* $C_{\phi_{2l}}$, $C_{\phi_{3l}}$ *and* $C_{\theta_{3l}}$ *are the lth diagonal elements of* C_{ϕ_2}, C_{ϕ_3} *and* C_{θ_3}, *respectively. Then, the control law* (29) *guarantees that*:

A. *In general, the control input is bounded and the closed-loop system is globally stable with V bounded above by*

$$V(t) \leqslant \exp(-\lambda_V t)V(0) + \frac{\varepsilon_V}{\lambda_V}[1 - \exp(-\lambda_V t)], \tag{34}$$

where $\lambda_V = 2\min\{k_2, k_3\}$ *and* $\varepsilon_V = w_2\varepsilon_2 + w_3\varepsilon_3$.

B. *If after a finite time* t_0, $\tilde{\boldsymbol{d}} = 0$, *i.e., in the presence of parametric uncertainties only, then, in addition to results in A, asymptotic output tracking (or zero final tracking error) is also achieved.* △

Proof. Proof of the Theorem is given in Appendix A.

Remark 3. Results in A of Theorem 1 indicate that the proposed controller has an exponentially converging transient performance with the exponentially converging rate λ_V and the final tracking error being able to be adjusted via certain controller parameters freely in a known form; it is seen from (34) that λ_V can be made arbitrarily large, and ε_V/λ_V, the bound of $V(\infty)$ (an index for the final tracking errors), can be made arbitrarily small by increasing feedback gains k_2 and k_3 and/or decreasing controller parameters ε_2 and ε_3. Such a guaranteed transient performance is especially important for the control of linear motors since execute time of a run is short. Theoretically, this result is what a well-designed robust controller can achieve. In fact, when the parameter adaptation law (12) is switched off, the proposed ARC law becomes a deterministic robust control law and Results A of the Theorem remain valid [9,11].

B of Theorem 1 implies that, compared to DRC, the proposed ARC achieves an improved tracking accuracy due to the reduced parametric uncertainties. Theoretically, Result B is what a well-designed adaptive controller can achieve. ♢

3.3. Desired trajectory initialization and generation

It is seen from (34) that transient tracking error is affected by the initial value $V(0)$, which may depend on the controller parameters also. To further reduce transient tracking error, the desired trajectory initialization can be used as follows. Namely, instead of simply letting the desired trajectory for the controller be the actual desired trajectory or position (i.e., $x_{1d}(t) = x_{Ld}(t)$), we can generate $x_{1d}(t)$ using a filter. For example, $x_{1d}(t)$ can be generated by the following third-order stable system

$$x_{1d}^{(3)} + \beta_1 x_{1d}^{(2)} + \beta_2 x_{1d}^{(1)} + \beta_3 x_{1d} = x_{Ld}^{(3)} + \beta_1 x_{Ld}^{(2)} + \beta_2 x_{1d}^{(1)} + \beta_3 x_{Ld}. \tag{35}$$

The initial conditions of the system (35) can be chosen to render $V(0) = 0$ to reduce transient tracking error.

Lemma 1. *If the initials* $x_{1d}(0), \ldots, x_{1d}^{(3)}(0)$ *are chosen as*

$$\begin{aligned} &x_{1d}(0) = x_1(0), \\ &\dot{x}_{1d}(0) = x_2(0), \\ &\ddot{x}_{1d}(0) = \{\hat{K}_F x_3 + \hat{\theta}_3 x_2 + \hat{\theta}_4 S_f(x_2) + \hat{\theta}_{5b}^T S_c(x_1) + \hat{\theta}_6\}\,|_{t=0}, \end{aligned} \tag{36}$$

then, $e_1(0) = 0, z_i(0) = 0, i = 2, 3$ *and* $V(0) = 0$.

Proof. The Lemma can be proved in the same way as in [11]. □

Remark 4. It is seen from (36) that the above trajectory initialization is independent from the choice of controller parameters such as $k = [k_2, k_3]^T$ and $\varepsilon = [\varepsilon_2, \varepsilon_3]^T$. Thus, once the initial position of the linear motor is determined, the above trajectory initialization can be performed off-line. ♢

Remark 5. By using the trajectory initialization (36), $V(0) = 0$. Thus, from (34), the controller output tracking error $e_1 = x_1 - x_{1d}$ is within a ball whose size can be made arbitrarily small by increasing k and/or decreasing ε in a known form. From (35) and (36), the trajectory planning error, $e_d(t) = x_{1d}(t) - x_{Ld}(t)$, can be guaranteed to possess any good transient behavior by suitably choosing the Hurwitz polynomial $G_d(s) = s^3 + \beta_1 s^2 + \beta_2 s + \beta_3$ and is known in advance. Therefore, any prescribed transient performance of the actual output tracking error $e_y = e_1(t) + e_d(t)$ can be achieved by selecting controller parameters properly. ♢

4. Simulation results

To illustrate the above designs, simulation results are obtained for a linear motor system shown in Fig. 1 with motor physical parameters obtained from the specifications of the iron-core LCK-S-1 linear motor by Anorad Company [18]. Nominal values of the system are: an inertia of $M = 10$ kg, a damping coefficient of $B = 0.5$ N/m/s, a motor back EMF of $K_E = 18.5$ V/m/s, a force constant of $K_{F_0} = 55.5$ N/A, a coil resistance of $R = 3.9\ \Omega$, an inductance of $L = 30$ mH, and a magnet pitch of $P = 30$ mm. The actual friction force used for simulation is given by (2), where $f_s = 10$, $f_c = 6$, $\dot{x}_s = 0.001$ and $\xi = 1$.

The following situation is considered: the shape function for friction compensation is chosen as $S_f(x_2) = \tanh(1000x_2)$ and the friction amplitude A_f is assumed to vary from 5 to 10 N. Cogging amplitude is assumed to be any value less than 30 N, and the amplitude of $K_{F_x}(x_1)$ is less than 1.11 N/A. For simplicity, in the simulation, only the first harmonics are used in the controller to approximate the periodic cogging force and $K_{F_x}(x_1)$, i.e., $q_1 = q_2 = 1$ in (6). Other parameter variations are as following: $M = 5$–30 kg, $B = 0.2$–0.7 N/m/s, $K_E = 15$–20 V/m/s, $R = 2$–$5\ \Omega$, $L = 20$–40 mH and $\tilde{f} = -40$–40 N. As such, the bounds describing the uncertain ranges in (10) are given by $\theta_{\min} = [1.85, -0.22, -0.22, -0.14, 0.17, -6, -6, -8, 25, -250, -1000]^T$, $\theta_{\max} = [11.1, 0.22, 0.22, -0.0067, 2, 6, 6, 8, 50, -50, -375]^T$, and $\delta_d = 3$. The initial parameter estimates are $\hat{\theta} = [1.85, 0, 0, -0.1, 1.67, 0, 0, 0, 31.25, -133, -667]^T$, which are different from the nominal values of $\theta = [5.55, 0.089, 0.089, -0.05, 0.6, 1.5, 1.5, 0, 33.3, -130, -616.7]^T$ to test the effect of parametric uncertainties. A sampling rate of 0.2 ms is used in the simulation. The following two controllers are compared:

- ARC: The proposed ARC law with the discontinuous projection synthesized in Section 3. The controller parameters are: $k_p = 200$, $k_{2s1} = 200$, $w_2 = 1$, $\varepsilon_2 =$

5×10^4; $k_{3s1} = 300$, $w_3 = 0.1$, $\varepsilon_3 = 1 \times 10^7$. The adaptation rate matrix is $\Gamma = \mathbf{diag}[342, 0.39, 0.39, 3.5 \times 10^{-3}, 0.67, 288, 288, 51.2, 125, 8 \times 10^3, 7.8 \times 10^4]$. Trajectory planning parameters are $\beta_1 = 120$, $\beta_2 = 4800$ and $\beta_3 = 64\,000$, respectively.

- DRC: Deterministic robust control – the same control law as the above ARC but without using parameter adaptation.

To test the tracking capability of the proposed algorithm, a sinusoidal desired trajectory given by $x_{Ld} = 0.01\sin(2\pi t)$ and the trajectory initialization (36) are used. To show the nominal learning capability of the proposed ARC, simulations are first run for the case when model uncertainties are dominated by parametric uncertainties as follows. Actual cogging force $f_{\text{cogging}}(x_1)$ and the position-dependent force constant K_{F_x} used for plant simulation are assumed to be of first harmonics only, i.e., $F_{\text{cogging}} = 25\sin(2\pi x_1/P + \pi/4)$ and $K_{Fx} = 1.11\sin(2\pi x_1/P + \pi/4)$, and there is no external disturbance ($f_{\text{dis}} = 0$). In such a case, the design models (6) are the same as their actual models to minimize the lumped disturbance (8). Thus, model uncertainties are mainly due to parametric uncertainties (Note that the magnitudes of the above cogging force and force ripples are assumed unknown and different initial estimates are used for controllers). Tracking errors are shown in Fig. 2. As seen, both controllers have very small tracking errors but the final errors of ARC are much smaller than that of DRC due to parameter adaptation.

The simulation is then run for the case that actual models of $f_{\text{cogging}}(x_1)$ and $K_{F_x}(x_1)$ are much different from their design models (6). Specifically, both $f_{\text{cogging}}(x_1)$ and $K_{F_x}(x_1)$ are assumed consisting of the first and the third harmonics [3] as $F_{\text{cogging}} = 15\sin(2\pi x_1/P + \pi/4) + 20\sin(6\pi x_1/P + 0.09\pi)$ and $K_{F_x} =$

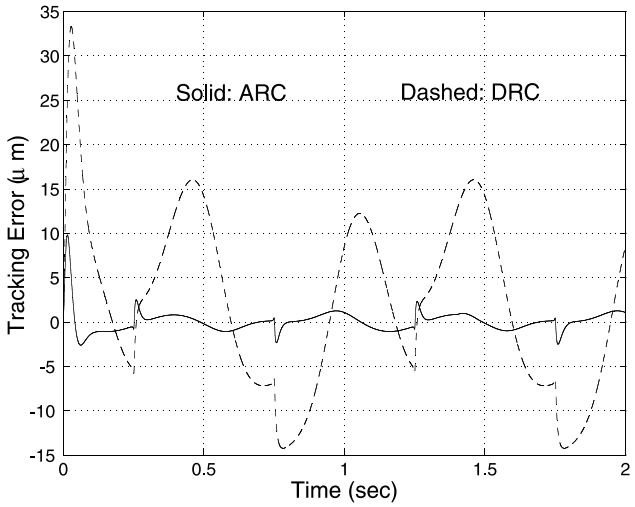

Fig. 2. Tracking errors in the presence of parametric uncertainty.

$K_{F_0}(0.016\sin(2\pi x_1/P + \pi/4) + 0.02\sin(6\pi x_1/P + 0.09\pi))$. Tracking errors are shown in Fig. 3. As seen, the large mismatch between the design models and the actual models for ripple forces does not degrade the performance of the proposed ARC much. This verifies the performance robustness of the proposed ARC to uncompensated uncertain nonlinearities.

To test performance robustness of the proposed ARC to external disturbances, an external disturbance force $f_{\text{dis}} = 30 + 5\ rand$ (N) is then added to the system during the period $0 < t < 1$ s. Tracking errors are shown in Fig. 4. As seen, during the period of the appearance of external disturbance (the first second), tracking error is the almost same level as that without external disturbance. This is because that the proposed ARC can adapt to the nominal value of the lumped disturbance (θ_6) very quickly. Compared to non-adapting DRC design, the proposed ARC achieves a much better tracking accuracy.

The simulation is also run for fast-changing desired trajectories and similar trends have been observed. For example, for a 4 Hz desired trajectory given by $x_{Ld} = 0.01\sin(8\pi t)$, tracking errors shown in Fig 5 are very small and exhibit similar trends as in Fig. 2.

The simulation results of the above tests are also measured in terms of several performance indexes quantitatively, which are summarized in Table 1. The maximum absolute value of the tracking error $e_{\text{M}} = \max\{|e_1(t)|\}$, is used as an index of *transient performance*. The maximum absolute value of the tracking error during the last 0.5 s, $e_{\text{F}} = \max_{1.5 \leqslant t \leqslant 2}\{|e_1(t)|\}$, is used as an index of *final tracking accuracy*. The rms value of the tracking error $\|e_{\text{rms}}\| = (1/T\int_0^T e_1(t)^2\,\mathrm{d}t)^{1/2}$, is used to measure *average tracking performance*,

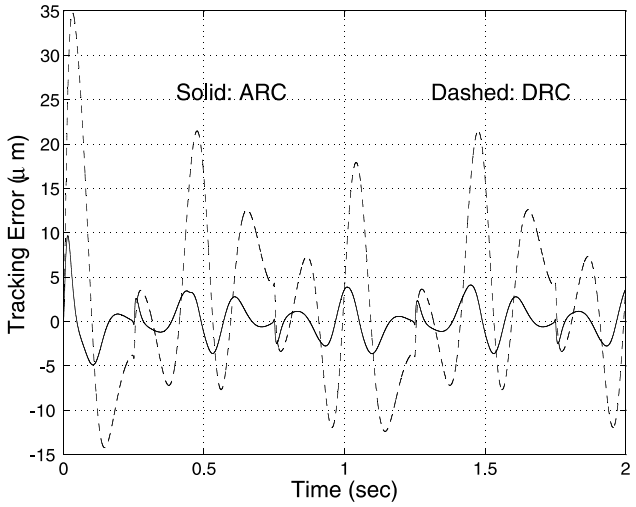

Fig. 3. Tracking errors with model mismatch.

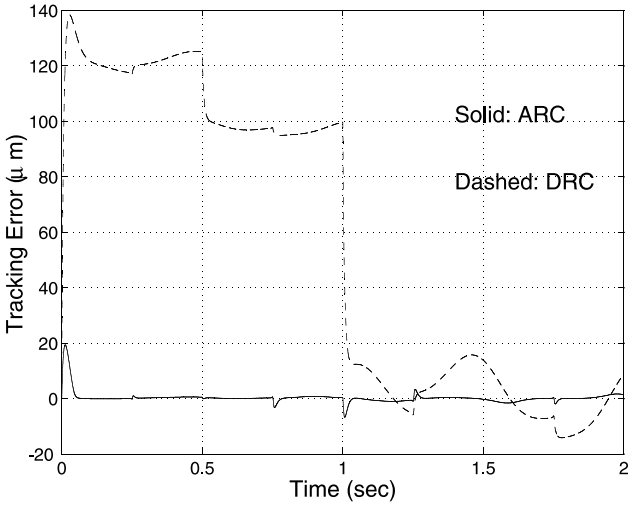

Fig. 4. Tracking errors in the presence of parametric uncertainty and external disturbances.

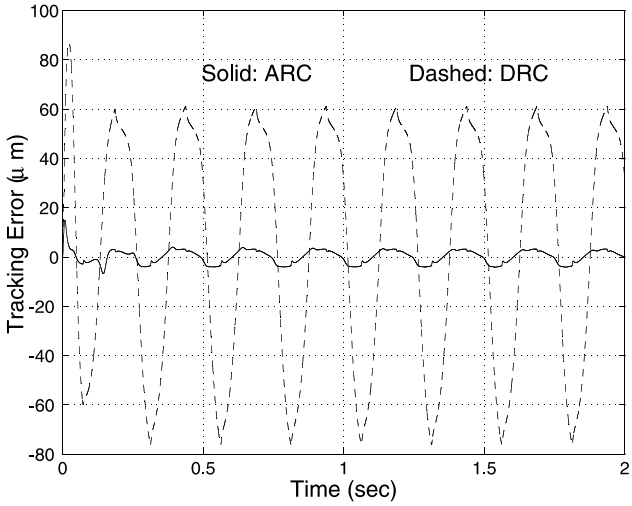

Fig. 5. Tracking errors for a higher frequency desired trajectory.

Finally, simulation is run for point-to-point movement of the linear motor. Given the start and the final position of the motor, a desired trajectory $x_{Ld}(t)$ with a continuous velocity and acceleration is first planned. For a travel distance of 0.4 m, the planned $x_{Ld}(t)$ and $\dot{x}_{Ld}(t)$ are shown in Fig. 6. As seen, the desired trajectory has a maximum speed of 2 m/s and has a maximum acceleration of 20 m/s^2, which are around their physical limits. An adaptation rate of $\Gamma = \mathbf{diag}[342, 0.39, 0.39, 3.5 \times 10^{-5}, 6.7 \times 10^{-3}, 288, 288, 0.51, 1.25, 80, 7.8 \times 10^2]$ is used. Tracking errors are shown in Fig 7. As seen, due to large acceleration and very high speed during

Table 1
Summary of the simulation results measured quantitatively in terms of several performance indexes

Controller	Fig. 2		Fig. 3		Fig. 4		Fig. 5	
	DRC	ARC	DRC	ARC	DRC	ARC	DRC	ARC
e_M (μm)	33.3	9.81	34.8	9.66	138	19.4	86.9	14.9
e_F (μm)	14.2	2.49	11.9	3.62	14.1	1.88	76.1	4.06
$\|e_{rms}\|$ (μm)	10.0	1.26	10.0	2.12	78.6	2.16	49.2	2.81

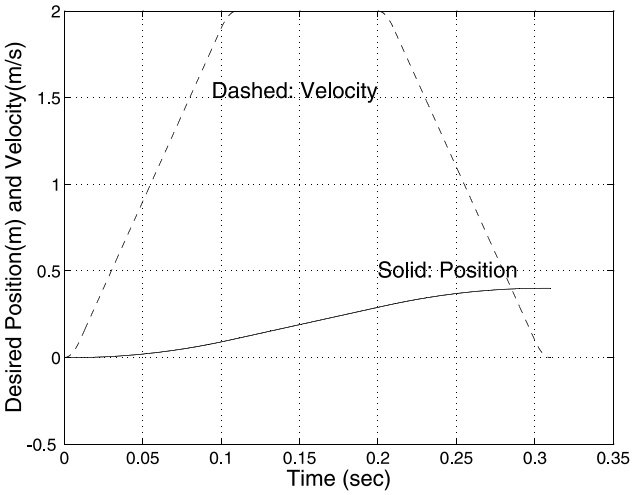

Fig. 6. Desired trajectory and velocity for a travel distance of 0.4 m.

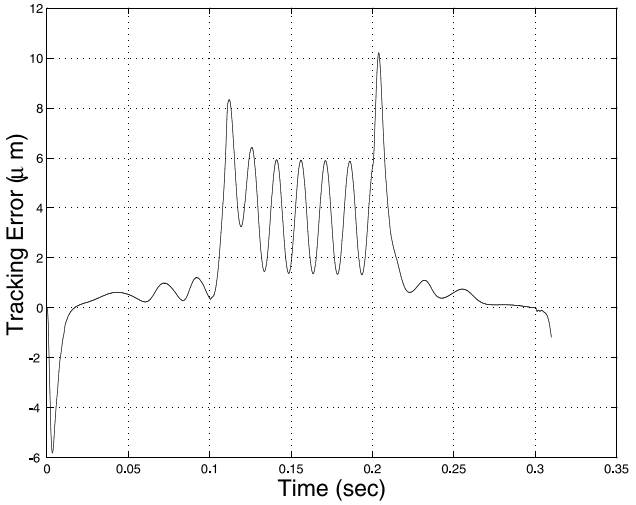

Fig. 7. Tracking error of the whole travel distance.

transient period, transient tracking error becomes larger but the final tracking error is only 1.4 μm. It is interesting to note that during the maximum speed period (around 0.1–0.21 s), ripple forces have a frequency of 2 ms/0.03 m = 66.67 Hz, which is beyond the bandwidth of the controller. As a result, parameter adaptation could not catch the periodic ripple forces and their effects are evident in the transient tracking error. The results also show that the proposed ARC is robust to very high frequency ripple forces as contrast to the instability phenomenon observed in other learning techniques [6]. All these results verify the effectiveness of the proposed algorithm.

5. Conclusions

In this paper, an ARC controller based on discontinuous projection method has been constructed for the high-performance adaptive robust motion control of an iron-core linear motor. The controller takes into account the effect of parametric uncertainties coming from the inertia load, friction, cogging, force ripple, and electrical parameters as well as uncertain nonlinearities due to external disturbances, uncompensated friction and force ripple. In particular, design models consisting of known basis functions with unknown weights are used to approximate the unknown nonlinear ripple forces. On-line parameter adaptation is then utilized to reduce the effect of various parametric uncertainties while the uncompensated uncertain nonlinearities are handled effectively via certain robust control laws for high performance. As a result, time-consuming and costly rigorous off-line identification of friction and ripple forces is avoided while without sacrificing tracking performance. Extensive simulation results illustrated the effectiveness of the proposed scheme – a fast parameter adaptation process, performance robustness to uncompensated model errors and external disturbances, and robust to very high frequency ripple forces.

Acknowledgements

Part of the paper has been presented in the 1999 IFAC World Congress. The work is supported by the National Science Foundation under the CAREER grant CMS-9734345. The authors would like to thank Dr. Y. Shin for helpful discussions on the subject.

Appendix A

Proof of Theorem 1. Substituting (29) into (30) and noting (19) and (21)

$$\begin{aligned}\dot{V} \leqslant\ & w_2 z_2 \left\{ \bar{K}_F \alpha_{2s2} - \tilde{\theta}^T \phi_2 + \tilde{d} \right\} - w_2 \frac{\bar{K}_F}{K_{F_{\min}}} (k_2 + \|C_{\phi_2} \Gamma \phi_2\|^2) z_2^2 \\ & + w_3 z_3 \left(\theta_7 u_{s2} - \tilde{\theta}^T \phi_3 - \frac{\partial \alpha_2}{\partial x 2} \tilde{d} \right) - w_3 \frac{\theta_7}{\theta_{7\min}} \left(k_3 + \left\| \frac{\partial \alpha_2}{\partial \hat{\theta}} C_{\theta_3} \right\|^2 + \|C_{\phi_3} \Gamma \phi_3\|^2 \right) z_3^2 \\ & - w_3 z_3 \frac{\partial \alpha_2}{\partial \hat{\theta}} \dot{\hat{\theta}}. \end{aligned} \tag{A.1}$$

By completion of square

$$\left|w_3 z_3 \frac{\partial \alpha_2}{\partial \hat{\theta}} \dot{\hat{\theta}}\right| \leqslant w_3 \left\| \frac{\partial \alpha_2}{\partial \hat{\theta}} C_{\theta_3} C_{\theta_3}^{-1} \dot{\hat{\theta}} \right\| z_3 \Bigg| \leqslant w_3 \left\| \frac{\partial \alpha_2}{\partial \hat{\theta}} C_{\theta_3} \right\|^2 z_3^2 + \frac{w_3}{4} \left\| C_{\theta_3}^{-1} \dot{\hat{\theta}} \right\|^2. \tag{A.2}$$

Noting that $C_{\theta_3}^{-1}$ and Γ are diagonal matrices, from (12) and (33),

$$\begin{aligned} \left\| C_{\theta_3}^{-1} \dot{\hat{\theta}} \right\|^2 &= \| C_{\theta_3}^{-1} \mathrm{Proj}_{\hat{\theta}}(\Gamma \tau) \|^2 \leqslant \| C_{\theta_3}^{-1} \Gamma \tau \|^2 \leqslant (\| C_{\theta_3}^{-1} \Gamma w_2 \phi_2 z_2 \| + \| C_{\theta_3}^{-1} \Gamma w_3 \phi_3 z_3 \|)^2 \\ &\leqslant 2(\| C_{\theta_3}^{-1} \Gamma \phi_2 \|^2 w_2^2 z_2^2 + \| C_{\theta_3}^{-1} \Gamma \phi_3 \|^2 w_3^2 z_3^2). \end{aligned} \tag{A.3}$$

Thus, if C_{ϕ_2}, C_{ϕ_3}, and C_{θ_3} satisfy the conditions in the theorem, from (A.2) and (A.3),

$$\begin{aligned} \left| w_3 z_3 \frac{\partial \alpha_2}{\partial \hat{\theta}} \dot{\hat{\theta}} \right| &\leqslant w_3 \left\| \frac{\partial \alpha_2}{\partial \hat{\theta}} C_{\theta_3} \right\|^2 z_3^2 + \frac{1}{2} w_3 (\| C_{\theta_3}^{-1} \Gamma \phi_2 \|^2 w_2^2 z_2^2 + \| C_{\theta_3}^{-1} \Gamma \phi_3 \|^2 w_3^2 z_3^2) \\ &\leqslant w_3 \left\| \frac{\partial \alpha_2}{\partial \hat{\theta}} C_{\theta_3} \right\|^2 z_3^2 + w_2 \| C_{\phi_2} \Gamma \phi_2 \|^2 z_2^2 + w_3 \| C_{\phi_3} \Gamma \phi_3 \|^2 z_3^2. \end{aligned} \tag{A.4}$$

Noting the conditions (i) of (22) and (31), from (A.1) and (A.4),

$$\dot{V} \leqslant \sum_{j=2}^{3} (-w_j k_j z_j^2 + w_j \varepsilon_j) \leqslant -2\lambda_V V + \varepsilon_V \tag{A.5}$$

which leads to (34). A of the theorem is thus proved.In the presence of parametric uncertainties only, i.e., $\tilde{d} = 0$, noting conditions (ii) of (22) and (31), from (A.1), (A.4), and (33),

$$\dot{V} \leqslant -\sum_{j=2}^{3} \left[w_j \tilde{\theta}^T \phi_j z_j + w_j k_j z_j^2 \right] = -\sum_{j=2}^{3} w_j k_j z_j^2 - \tilde{\theta}^T \tau. \tag{A.6}$$

Define a new pdf V_θ as

$$V_\theta = V + \frac{1}{2} \tilde{\theta}^T \Gamma^{-1} \tilde{\theta}. \tag{A.7}$$

Noting P2 of (13), from (A.6), the derivative of V_θ is

$$\dot{V}_\theta \leqslant -\sum_{j=2}^{3} w_j k_j z_j^2 - \tilde{\theta}^T \tau + \tilde{\theta}^T \Gamma^{-1} \dot{\hat{\theta}} \leqslant -\sum_{j=2}^{3} w_j k_j z_j^2. \tag{A.8}$$

Therefore, $z \in L_2^2$. It is also easy to check that $\dot{z}$ is bounded. So, $z \to 0$ as $t \to \infty$ by the Barbalat's lemma, which leads to B of Theorem 1. □

References

[1] Alter DM, Tsao TC. Control of linear motors for machine tool feed drives: design and implementation of H_∞ optimal feedback control. ASME J Dyn Syst, Meas, Control 1996;118:649–56.
[2] Alter DM, Tsao TC. Dynamic stiffness enhancement of direct linear motor feed drives for machining. In: Proceedings of the American Control Conference, 1994. p. 3303–7.

[3] Braembussche PV, Swevers J, Brussel HV, Vanherck P. Accurate tracking control of linear synchronous motor machine tool axes. Mechatronics 1996;6(5):507–21.
[4] Komada S, Ishida M, Ohnishi K, Hori T. Disturbance observer-based motion control of direct drive motors. IEEE Trans Energy Convers 1991;6(3):553–9.
[5] Egami T, Tsuchiya T. Disturbance suppression control with preview action of linear DC brushless motor. IEEE Trans Ind Electron 1995;42(5):494–500.
[6] Otten G, Vries T, Amerongen J, Rankers A, Gaal E. Linear motor motion control using a learning feedforward controller. IEEE/ASME Trans Mechatronics 1997;2(3):179–87.
[7] Ohnishi K, Shibata M, Murakami T. Motion control for advanced mechatronics. IEEE/ASME Trans Mechatronics 1996;1(1):56–67.
[8] Yao B, Al-Majed M, Tomizuka M. High performance robust motion control of machine tools: an adaptive robust control approach and comparative experiments. IEEE/ASME Trans Mechatronics 1997;2(2):63–76 (Part of the paper also appeared in Proceedings of the 1997 American Control Conference).
[9] Yao B, Tomizuka M. Smooth robust adaptive sliding mode control of robot manipulators with guaranteed transient performance. In: Proceedings of the American Control Conference, 1994. p.1176–80. (The full paper appeared in ASME J Dynamic Syst, Meas Control 1996;118(4):764–75.)
[10] Yao B, Tomizuka M. Comparative experiments of robust and adaptive control with new robust adaptive controllers for robot manipulators. In: Proceedings of the IEEE Conference on Decision and Control; 1994. p. 1290–5.
[11] Yao B, Tomizuka M. Adaptive robust control of SISO nonlinear systems in a semi-strict feedback form. Automatica 1997;33(5):893–900. (Part of the paper appeared in Proceedings of the 1995 American Control Conference. p. 2500–5).
[12] Yao B, Tomizuka M. Adaptive robust control of MIMO nonlinear systems in semi-strict feedback forms, 1999. Submitted to Automatica (revised in 1999 and conditionally accepted) (Parts of the paper were presented in the IEEE Conference on Decision and Control, 1995, p. 2346–51 and the IFAC World Congress, 1996, Vol. F, p. 335–40.
[13] Slotine JJE, Li W. Adaptive manipulator control: a case study. IEEE Trans Autom Control 1988;33(11):995–1003.
[14] Krstic M, Kanellakopoulos I, Kokotovic PV. Nonlinear and adaptive control design. New York: Wiley, 1995.
[15] Utkin VI. Sliding modes in control optimization. Berlin: Springer Verlag, 1992.
[16] Corless MJ, Leitmann G. Continuous state feedback guaranteeing uniform ultimate boundedness for uncertain dynamic systems. IEEE Trans Autom Control 1981;26(10):1139–44.
[17] Yao B. High performance adaptive robust control of nonlinear systems: a general framework and new schemes. In: Proceedings of the IEEE Conference on Decision and Control, 1997. p. 2489–94.
[18] Anorad Linear Motors. 110 Oser Avenue, Hauppauge, NY11788: Anorad Corporation; 1997.
[19] Canudas de Wit C, Olsson H, Astrom KJ, Lischinsky S. A new model for control of systems with friction. IEEE Trans Autom Control 1995;40(3):419–25.
[20] Armstrong-Helourry B, Dupont P, Canudas de Wit C. A survey of models analysis tools and compensation methods for the control of machines with friction. Automatica 1994;30(7):1083–138.
[21] Krause PC. Analysis of electric machinery. New York: McGraw-Hill, 1986.
[22] Le-Huy H, Perret R, Feuillet R. Minimization of torque ripple in brushless DC motor drives. IEEE Trans Ind Appl 1986;22(4):748–55.
[23] Hanselman DC. Brushless permanent-magnet motor design. New York: McGraw-Hill, 1994.
[24] Yao B, Tomizuka M. Smooth robust adaptive sliding mode control of robot manipulators with guaranteed transient performance. Trans J Dyn Syst, Meas, Control 1996;118(4):764–775 (Part of the paper also appeared in the Proceedings of the 1994 American Control Conference).
[25] Lee HS, Tomizuka M. Robust motion controller design for high-accuracy positioning systems. IEEE Trans Ind Electron 1996;43(1):48–55.

[26] Sastry S, Bodson M. Adaptive control: stability convergence and robustness. Englewood Cliffs, NJ: Prentice Hall, 1989.
[27] Goodwin GC, Mayne DQ. A parameter estimation perspective of continuous time model reference adaptive control. Automatica 1989;23(1):57–70.